



HAL
open science

Influence of π -electron conjugation outside the aromatic ring on the methyl internal rotation of 4-methyl-5-vinylthiazole

Safa Khemissi, Martin Schwell, Isabelle Kleiner, Ha Vinh Lam Nguyen

► **To cite this version:**

Safa Khemissi, Martin Schwell, Isabelle Kleiner, Ha Vinh Lam Nguyen. Influence of π -electron conjugation outside the aromatic ring on the methyl internal rotation of 4-methyl-5-vinylthiazole. *Molecular Physics*, 2022, pp.e2052372. 10.1080/00268976.2022.2052372 . hal-03631735

HAL Id: hal-03631735

<https://hal.u-pec.fr/hal-03631735>

Submitted on 5 Apr 2022

HAL is a multi-disciplinary open access archive for the deposit and dissemination of scientific research documents, whether they are published or not. The documents may come from teaching and research institutions in France or abroad, or from public or private research centers.

L'archive ouverte pluridisciplinaire **HAL**, est destinée au dépôt et à la diffusion de documents scientifiques de niveau recherche, publiés ou non, émanant des établissements d'enseignement et de recherche français ou étrangers, des laboratoires publics ou privés.

Influence of π -electron conjugation outside the aromatic ring on the methyl internal rotation of 4-methyl-5-vinylthiazole

Special issue HRMS Jean-Marie Flaud

Safa Khemissi^a, Martin Schwell^a, Isabelle Kleiner^b and Ha Vinh Lam Nguyen^{a,c*}

^a *Univ Paris Est Creteil and Université de Paris, CNRS, LISA, F-94010 Créteil, France*

^b *Université de Paris and Univ Paris Est Creteil, CNRS, LISA, F-75013 Paris, France*

^c *Institut Universitaire de France (IUF), F-75231 Paris, France*

* Corresponding author:

Ha Vinh Lam Nguyen

Univ Paris Est Creteil and Université de Paris, CNRS, LISA, F-94010 Créteil, France

Institut Universitaire de France (IUF), F-75231 Paris, France

Email: lam.nguyen@lisa.ipsl.fr

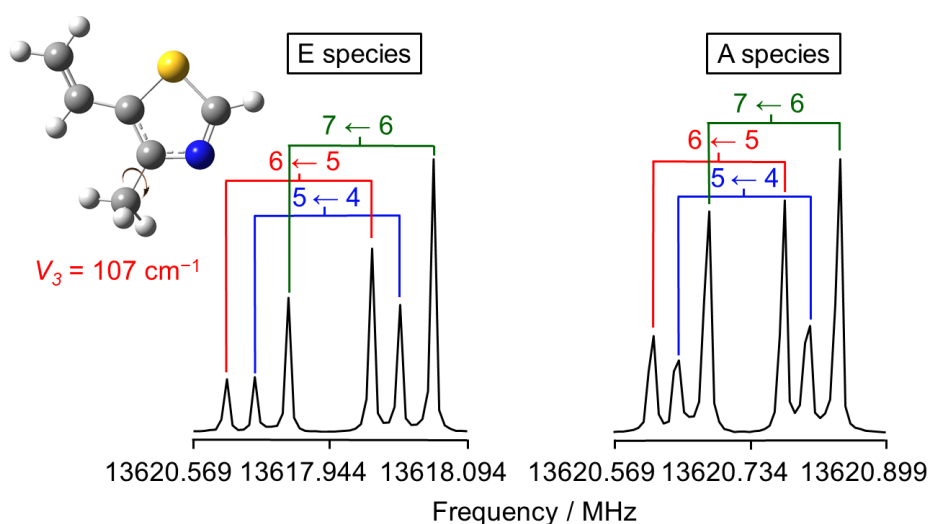
Influence of π -electron conjugation outside the aromatic ring on the methyl internal rotation of 4-methyl-5-vinylthiazole

Abstract

The microwave spectrum of 4-methyl-5-vinylthiazole was measured using a pulsed molecular jet Fourier transform microwave spectrometer operating in the frequency range from 2.0 to 26.5 GHz. Only the *anti*-conformer was observed. Due to internal rotation of the methyl group, doublets containing an A and an E torsional species were found for all rotational transitions. Hyperfine structures arising from the ^{14}N nuclear quadrupole coupling were resolved. The complex spectral patterns were analysed and fitted using the *XIAM* and *BELGI-C_s-hyperfine* codes, yielding a barrier to methyl internal rotation of $107.0901(7) \text{ cm}^{-1}$ and the quadrupole coupling constants $\chi_{aa} = -3.545(13)$, $\chi_{bb} - \chi_{cc} = -1.563(24)$ and $\chi_{ab} = -1.76(11) \text{ MHz}$. The experimental results were supported by data from quantum chemistry. Some calculations using the MP2 method yielded non-planar structures, where the vinyl group is tilted out of the thiazole ring plane. The inertial defect and the χ_{cc} constant were compared with those obtained for other aromatic molecules to support the planarity of the 4-methyl-5-vinylthiazole. A comparison of the methyl torsional barrier with other thiazole derivatives suggests that electrostatic effects caused by the π -conjugated system of thiazole extended by the vinyl group are the reason of the low torsional barrier of the methyl group.

Keywords: rotational spectroscopy, internal rotation, nuclear quadrupole coupling, microwave spectroscopy.

Graphical abstract



Dedication

It is an honour to contribute to the special issue dedicated to the 27th Colloquium on High-Resolution Molecular Spectroscopy (HRMS 2021), and especially to Dr. Jean-Marie Flaud on the occasion of his 75th birthday. Dr. Flaud offered to many young researchers a chance to join the spectroscopic community and mentored them with a lot of freedom to explore various domains. We wish him a happy birthday.

Introduction

Thiazole and its derivatives form one of the most important classes of five-membered heterocycles. Their molecular structures and characterizations are therefore of particular interest. The first study on thiazole by Bak et al. [1] goes back to 1962, where the dipole moment of the ground state was determined alongside with the rotational constants. A recent investigation by Esselman et al. [2] revealed the molecular structure of thiazole using millimetre-wave spectroscopy supported by quantum chemical calculations. Among the derivatives of thiazole, we particularly interested in methylthiazole. The methyl group undergoes a large amplitude motion (LAM) called internal rotation, which causes all rotational lines present in the experimental spectrum to split into doublets, making the spectral assignment and modelling more challenging compared to a rigid-rotor case [3]. The separations of these so-called A-E doublets depend on the barrier hindering the methyl torsion, whose value in turn depends on several aspects such as steric hindrance and electrostatic effects. Many studies on aromatic five- and six-membered rings have shown the impact of steric hindrance on methyl torsional barriers, e.g. 2,6- (237 cm⁻¹) and 3,4-dimethylfluorobenzene (456 and 490 cm⁻¹) [4,5], 3,4-dimethylbenzaldehyde (450 and 550 cm⁻¹) [6], 3,4-dimethylanisole (430 and 467 cm⁻¹) [7], 2,5-dimethylpyrrole (317 cm⁻¹) [8] and 2,5-dimethylthiophene (248 cm⁻¹) [9], where the barriers heights are intermediate due to steric hindrance arising from an atom or a group adjacent to the methyl top. However, steric effects fail to explain the unexpectedly lower barrier to internal rotation of the *o*-methyl group in 2,3-dimethylfluorobenzene (216 cm⁻¹) [10] and 2,3-dimethylanisole (27 cm⁻¹) [11], such that electrostatic effects in the π -conjugated system might be the origin. Similar observations were found for the two neighbouring methyl groups in 4,5-dimethylthiazole (127 and 62 cm⁻¹) [12] and the methyl group in 2-methylthiazole (35 cm⁻¹) [13].

If a substitution with a double bond is attached to the aromatic ring, the π -conjugated system is extended and π -electrons can “escape” from the ring through conjugation. In such

cases, the methyl rotor is extremely sensitive to other substituents or components of the aromatic ring, as the π -electrons can transfer information through the whole molecule. This “long distance calling” [14] has been reported for many aromatic rings containing a carbonyl substituent and a methyl group attached to the ring such as *m*- [15] and *p*-tolualdehyde [14], *m*- [16] and *p*-toluic acid [17], 4-methylacetophenone [18], 5-methylfurfural [19], and 2-acetyl-5-methylfuran [20]. However, to the best of our knowledge, the effect of extended π -conjugations outside an aromatic ring by a C=C double bond has never been explored. Therefore, we were interested in 4-methyl-5-vinylthiazole (MVT) where the vinyl group at position five of the thiazole ring enables the π -electrons to be present outside the ring. A methyl group undergoing internal rotation is attached at position four. Since the methyl group is quite close to the adjacent vinyl group, we expected that the barrier to internal rotation will be intermediate (say $> 200 \text{ cm}^{-1}$). However, using Fourier transform microwave (FTMW) spectroscopy combined with quantum chemical calculations to determine this parameter, we found a much lower value which is inconsistent with hinderance arising by steric effects.

Not only the experimental value of the methyl torsional barrier of MVT was surprising, calculations of its equilibrium structures obtained at different levels of theory are also questionable. When a reliable structure determination using isotopic substitutions is not possible, quantum chemistry becomes an essential tool to supplement the microwave experiments. Though planarity seems to be obvious in conjugated double bond systems, we many times have to face the question “planar, or not planar”, as in the case of 2-propionylthiophene [21] or 2-acetyl-3-methylthiophene [22], as some MP2 levels of theory predict the carbonyl group to be tilted out of the aromatic ring by a small angle ($< 10^\circ$), while many other levels yield a planar structure. The same issue was observed for the vinyl group of MVT.

In addition, the thiazole ring contains a nitrogen atom with a nuclear spin of $I = 1$, causing all rotational lines to feature hyperfine splittings arising from ^{14}N nuclear quadrupole coupling effects. Though the quadrupole moment of the ^{14}N nucleus is small and can be treated with first order perturbation approximations, the combination of quadrupole hyperfine structures with the splittings arising from the methyl internal rotation with a relatively low barrier results in complicated spectral features, making the analysis of the microwave spectrum of MVT challenging.

In the present work, we measured the pulsed molecular jet FTMW spectrum of MVT and determined the molecular, internal rotation and ^{14}N nuclear quadrupole coupling parameters using quantum chemistry as a supporting tool. The results are compared with those of other

methyl top containing thiazole derivatives to yield insights into the concurrence between steric and electrostatic effects in this molecule.

Quantum chemical calculations

Conformational analysis

All quantum chemical calculations were carried out using the *Gaussian* 16 [23] program package. The structural optimizations were performed using the MP2 [24] and B3LYP-D3BJ [25-28] methods combined with Pople's 6-311++G(d,p) basis set [29]. The two methods were chosen because they had predicted rotational constants with sufficient accuracy to guide the experimental assignment in previous studies of many aromatic rings [19-22, 30].

We first performed a conformational analysis by varying the dihedral angle $\varphi = \angle(C_4, C_5, C_6, C_7)$ in a grid of 10° , i.e. rotating the vinyl group about the C_5-C_6 bond (see Figure 1 for atom numbering). All other molecular parameters were optimised. Due to symmetry, only a 180° rotation was necessary. With the thiazole ring being planar [2], we expected only two conformers with C_s symmetry due to π -conjugations and the vinyl group in a *syn* and in an *anti* orientation in relation to the methyl group. Surprisingly, the potential energy curves shown in Figure 2 and the parameterised Fourier coefficients given in Table S1 of the supplementary materials do not correspond to our expectation. With the MP2 method, two equivalent minima were predicted at 40° and 320° instead of the *syn* conformer at $\varphi = 0^\circ$, and a flat double minimum was calculated around 180° rather than the *anti* conformer. In calculations with the B3LYP-D3BJ method, the double minimum around $\varphi = 0^\circ$ was less pronounced, but did not vanish, while that around 180° disappears and $\varphi = 180^\circ$ is therefore predicted to be a stable conformer. Based on these results, B3LYP-D3BJ predicts a planar structure for the *anti* conformer and a non-planar structure for the *syn* conformer with the vinyl group tilted out of the thiazole ring by about 20° . The MP2 method calculates both conformers to be non-planar, where the vinyl tilt angle is about 20° for the *anti* conformer and 45° for the *syn* conformer. Note that in one of our previous studies on vinyl acetate, we observed a very similar behaviour of the potential curves (see Figure 6 of Ref. [31]), though the vinyl group is predicted to tilt out by smaller angles. Subsequently, full geometry optimisations were performed and the results are given in Table 1. The optimized structures of both conformers of MVT are illustrated in Figure 1. The atom Cartesian coordinates are given in Table S2 of the supplementary material. The *anti* conformer is the global minimum, being about 3.1 kJ/mol and 6.7 kJ/mol lower in energy than the *syn* conformer in MP2 and B3LYP-D3BJ calculations, respectively.

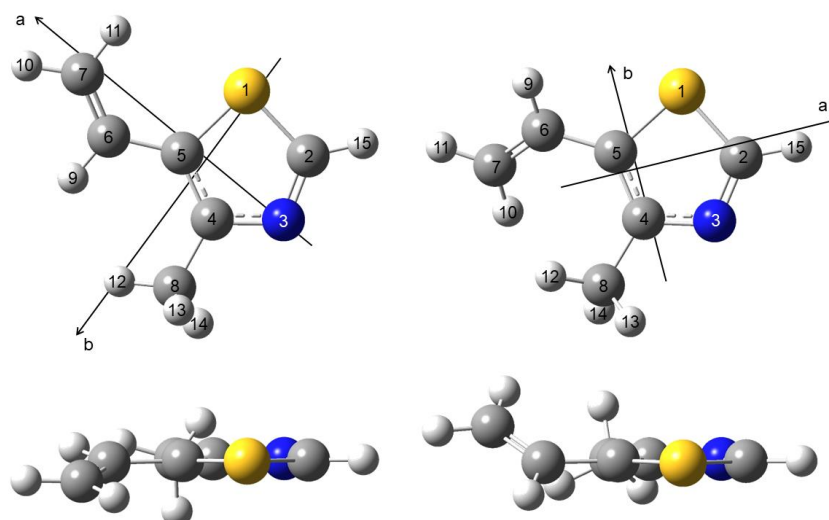


Figure 1. Optimised molecular structures of the *anti* and *syn* conformers of MVT obtained at the MP2/6-311++G(d,p) level of theory in their principal axis of inertia. The nitrogen atom is blue, sulphur yellow; the carbon atoms are grey and hydrogen atoms white. Upper trace: view onto the thiazole ring. Lower trace: view along the ring plane to visualise the tilt angle of the vinyl group.

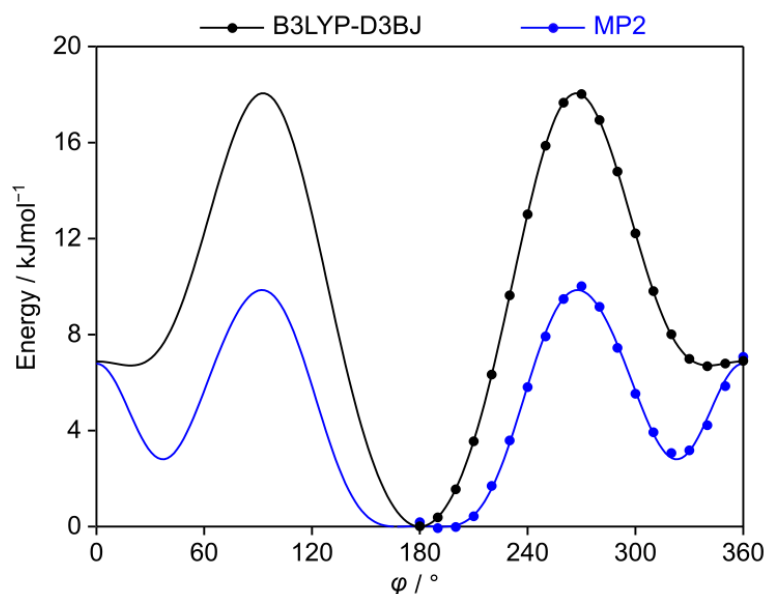


Figure 2. The potential energy curves obtained at the MP2/6-311++G(d,p) and B3LYP-D3BJ/6-311++G(d,p) levels of theory by varying the dihedral angle $\varphi = \angle(C_4, C_5, C_6, C_7)$ in 10° steps, corresponding to the rotation of the vinyl group. All other geometry parameters were optimised. The energies are given relative to the lowest values of -684.461659 Hartree (MP2) and -685.901835 Hartree (B3LYP-D3BJ).

Table 1. Equilibrium rotational constants, dipole moment components and relative energies of the *anti* and *syn* conformers of MVT calculated at the MP2/6-311++G(d,p) and B3LYP-D3BJ/6-311++G(d,p) levels of theory.

Par.	Unit.	MP2		B3LYP-D3BJ	
		<i>anti</i>	<i>syn</i>	<i>anti</i>	<i>syn</i>
A_e	MHz	2434.9	2667.3	2434.0	2693.2
B_e	MHz	1804.0	1699.1	1800.4	1683.6
C_e	MHz	1047.5	1064.9	1041.6	1048.7
$ \mu_a $	D	1.59	1.05	1.12	0.82
$ \mu_b $	D	0.06	1.37	0.18	1.00
$ \mu_c $	D	0.03	0.13	0.00	0.07
ΔE^a	kJ·mol ⁻¹	0.0	3.1	0.0	6.7

^a Energy differences are given relative to the lower energy conformer (*anti*-MVT) with $E = -684.4616729$ Hartree (MP2) and -685.9018345 Hartree (B3LYP-D3BJ).

Basis set variation

To assign rotational spectra, it is necessary to have a fairly reliable estimation of the rotational constants. The rapid development of modern quantum chemistry has made it possible to calculate equilibrium structures at affordable costs to access the rotational constants theoretically. To find out how reliable such predictions are, we calculated the rotational constants of the most stable *anti* conformer of MVT at different levels of theory to compare with the experimental ones. Density functional theory methods in use are B3LYP-D3, B3LYP-D3BJ, CAM-B3LYP [32], ω B97X-D [33] and M06-2X [34]; *ab initio* methods are MP2 and CCSD [35]. These methods were combined with several basis sets, such as Dunning’s polarized valence double- (cc-pVDZ) and triple-zeta (cc-pVTZ) [36], with or without diffuse functions included in the augmented basis sets known as aug-cc-pVDZ and aug-cc-pVTZ [37]. Pople’s basis sets [29] (6-31G or 6-311G) with or without diffuse (+ or ++) functions were also utilized with polarization functions like (d,p), (df,dp), (2d,2p), (2df,2pd), (3df,3dp) included in all cases. The predicted rotational constants are given in Table S3 of the supplementary materials. Regarding the planarity issue mentioned in Section ***Basis set variation***, the levels predicting a value of the tilt angle Θ significantly different from zero are bold in Table S3.

Methyl internal rotation

The barrier height to internal rotation of the methyl group was calculated at the MP2/6-311++G(d,p) and B3LYP-D3BJ/6-311++G(d,p) levels of theory for the energetically most stable conformer *anti*-MVT which was eventually observed in the microwave spectrum. We varied the dihedral angle $\alpha = \angle(\text{N}_3, \text{C}_4, \text{C}_8, \text{H}_{12})$ in steps of 10° in the range from 180° to 310° , which was sufficient taking into account the C_{3v} symmetry for the methyl group. All other parameters were optimised. The resulting energies were parameterised using a one-dimensional Fourier expansion with the obtained Fourier coefficients given in Table S4 of the supplementary materials. The potential energy curves are depicted in Figure 3. The V_3 potentials are 55.5 cm^{-1} (MP2) and 105.7 cm^{-1} (B3LYP-D3BJ).

A typical three-fold potential energy curve was obtained in calculations at the B3LYP-D3BJ/6-311++G(d,p) level of theory. In contrast, we found a non-symmetric shape with strange deformations at the MP2/6-311++G(d,p) level. This can be explained by the interaction of the methyl group during its rotation, causing the vinyl group to oscillate by up to 10° , as shown in the lower trace of Figure 3. In the B3LYP-D3BJ/6-311++G(d,p) calculations, the vinyl oscillation is almost negligible.

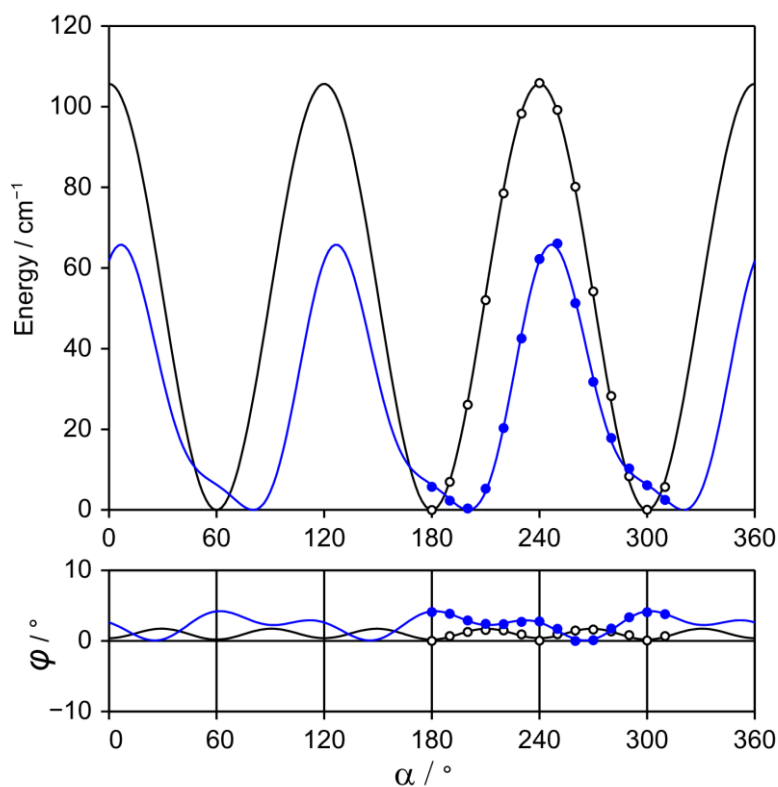


Figure 3. Upper trace: The potential energy curves for the methyl internal rotation calculated at the MP2/6-311++G(d,p) (blue curve) and B3LYP-D3BJ/6-311++G(d,p) (black curve) levels of theory. The

dihedral $\alpha = \angle(\text{N}_3, \text{C}_4, \text{C}_8, \text{H}_{12})$ was varied in steps of 10° . All other geometry parameters were optimised. The V_3 potentials are 55.5 cm^{-1} (MP2) and 105.7 cm^{-1} (B3LYP-D3BJ). The energies are given relative to the lowest energy conformations with $E = -684.461673$ Hartree (MP2) and -685.901835 Hartree (B3LYP-D3BJ). Lower trace: Oscillation of the vinyl group upon the rotation of the methyl group. The deviations of the dihedral φ are given relative to the smallest value $\varphi = 13.2065^\circ$ (MP2) and 0.0015° (B3LYP).

¹⁴N nuclear quadrupole coupling constants

The ¹⁴N nuclear quadrupole coupling constants (NQCCs) χ_{ij} reflect the splittings between the hyperfine components. They are proportional to the electronic field gradient (EFG) tensor components q_{ij} ($i, j = a, b, c$) at the quadrupole nucleus location.

$$\chi_{ij} = (eQ/h) q_{ij} \quad (1)$$

where e is the electron charge, Q the electric quadrupole moment of the nitrogen nucleus and h the Planck's constant. To calculate the EFG tensor from the structure optimised at the MP2/6-311++G(d,p) level of theory, the combination of the B3PW91 method and the 6-311+G(d,p) basis set was used with a calibration factor of $eQ/h = -4.599 \text{ MHz a.u.}^{-1}$, recommended for a molecule with a π -conjugated system [38], as introduced by Bailey [39]. The values of the NQCCs are $|\chi_{aa}| = 3.5525 \text{ MHz}$, $|\chi_{bb}| = 1.1313 \text{ MHz}$, $|\chi_{cc}| = 2.4211 \text{ MHz}$, $|\chi_{ab}| = 1.8195 \text{ MHz}$, $|\chi_{ac}| = 0.3125 \text{ MHz}$ and $|\chi_{bc}| = 0.1004 \text{ MHz}$.

Experiments

Measurements

The microwave spectrum of MVT was recorded between 2.0 and 26.5 GHz using a molecular jet FTMW spectrometer [40]. The substance with a stated purity of 98% was purchased from TCI Europe, Zwijndrecht, Belgium. Some drops of the sample were placed on a 6 cm piece of pipe cleaner inserted into a stainless steel tube placed upstream of the nozzle. Helium was passed over the sample at a backing pressure of 2 bar, before the helium-MVT mixture was expanded into the resonator chamber. We chose helium as carrier gas to observe higher J values with satisfactory intensity because the rotational cooling is not as effective as with neon or argon.

The microwave spectrum was measured using survey and the high-resolution modes of operation. At the beginning, we recorded a survey spectrum in the frequency range from 8.5 to 15.0 GHz by overlapping spectra with a frequency step of 0.25 MHz, which is the resolution of the scan. A portion of the scan from 11430 MHz to 11550 MHz is shown in Figure 4, where

lines are labelled by their assigned quantum numbers and symmetry species. Using the high-resolution mode with an experimental resolution of 2 kHz [41], lines obtained in the broadband survey were remeasured where doublets appear for all transitions due to the Doppler effect caused by the coaxial arrangement of the resonator and the molecular jet. A typical high-resolution spectrum of the $6_{06} \leftarrow 5_{05}$ rotational transition is shown in Figure 5. The estimated measurement accuracy is about 4 kHz, corresponding to 1/10 of the averaged full-width at half-maximum (FWHM).

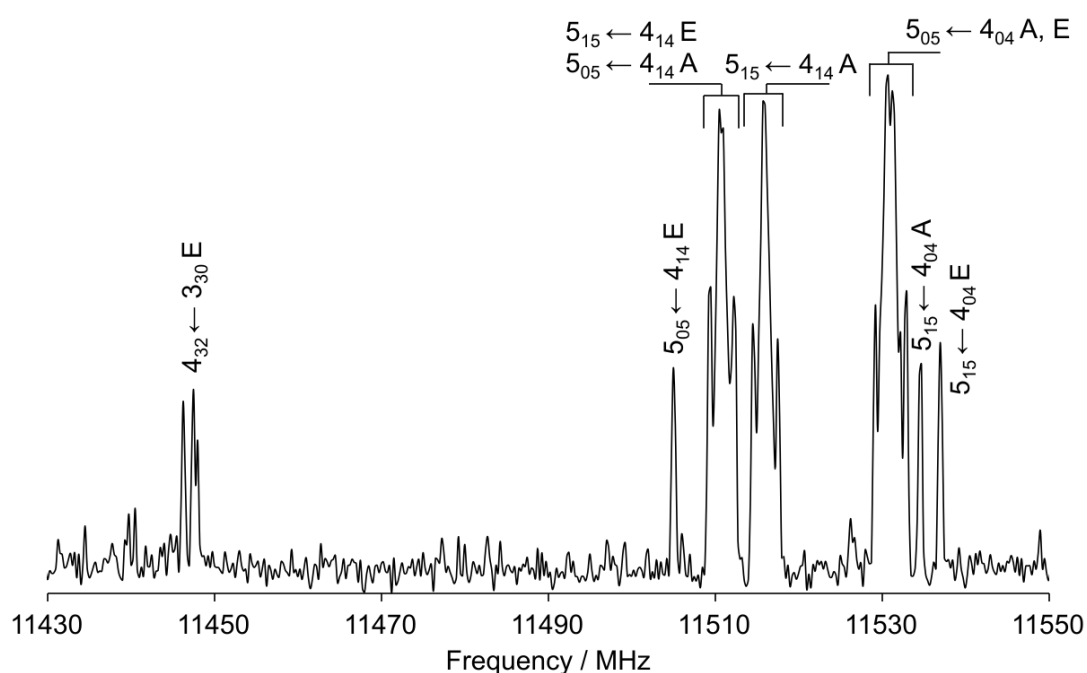


Figure 4. A portion of the broadband scan of MVT in the frequency range from 11430 to 11550 MHz recorded by overlapping spectra with 50 co-added decays per each spectrum. The arbitrary intensity is given in a logarithmic scale. All lines are marked with their assigned quantum numbers and symmetry species.

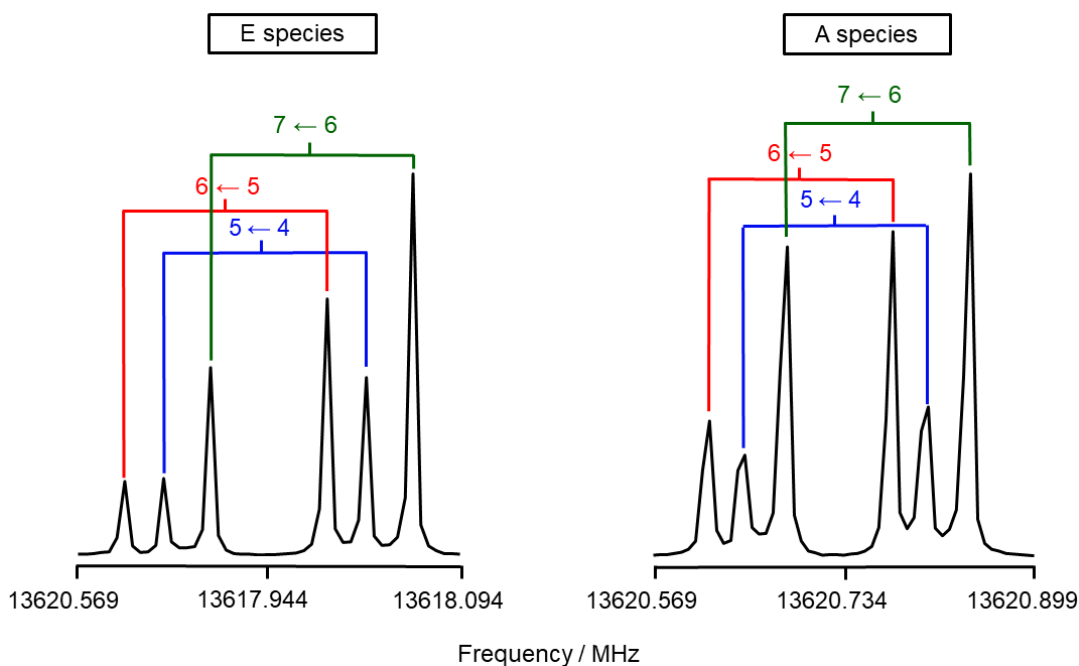


Figure 5. A typical high resolution spectrum of the *a*-type *R*-branch rotational transition $6_{06} \leftarrow 5_{05}$. The ^{14}N quadrupole hyperfine components are marked with the quantum numbers $F' \leftarrow F$. The Doppler components are connected by brackets. The A torsional species is on the right hand side and the E species on the left hand side.

Spectral assignment

We first started the spectral assignment with the more stable *anti* conformer. Using the rotational constants obtained at the MP2/6-311++G(d,p) level of theory given in Table 1, the theoretical rigid rotor spectrum of *anti*-MVT without the internal rotation and ^{14}N nuclear quadrupole coupling effects was predicted using the *XIAM* program [42] and compared to the survey spectrum. The calculated dipole moment components are $|\mu_a| = 1.59$ D, $|\mu_b| = 0.06$ D and $|\mu_c| = 0.03$ D. Therefore, only *a*-type transitions were expected. The intense *R*-branch *a*-type lines with $4 \leq J \leq 6$ are within the scan spectrum, and their frequencies are very well predicted. Assigning the rigid rotor spectrum was therefore straightforward. We then used the NQCCs calculated as described in section *^{14}N nuclear quadrupole coupling constants* to predict the hyperfine patterns. In the initial fit, a set of 78 A torsional symmetry species including their hyperfine splittings were fitted with a standard deviation of about 4 kHz, within the measurement accuracy. Using the fitted rotational constants and NQCCs, we predicted the rigid rotor transitions outside of the survey region, then measured and added new A species lines to the fit. The final A species fit contains 253 lines including hyperfine components, shown as Fit A in Table 2 with a standard deviation of 3.8 kHz.

The assignments of the E torsional symmetry species arising from the internal rotation of the methyl group was a challenge because of the relatively low barrier height of the methyl top. However, since the spectrum is dominated by *a*-type transitions, most of the A-E splittings are captured in the scan and could be assigned. Although the dipole moment component in the *b*-direction is predicted to be only 0.06 D, some *b*-type transitions were still observable. Some E-species *c*- and *x*-type transitions also appeared in the spectrum. The K_a and K_c quantum numbers have no meaning for those perturbation allowed transitions, because they only indicate the order of energy. We could finally assign 270 E species lines including their hyperfine components. The global *XIAM* fit achieved a standard deviation of 36.5 kHz. The obtained molecular parameters are listed as fit *XIAM* in Table 3.

The standard deviation of the *XIAM* fit is almost an order of magnitude larger than the measurement accuracy. Since it was not possible to check all assigned lines with combination different loops, the checking was done by separately fitting the A and E species including their hyperfine splittings using the program *WS18* [8]. The A species fit shown in Table 2 is essentially that obtained with the *XIAM* program. The Hamiltonian used to fit the E species lines with the *WS18* code is:

$$\mathbf{H} = \mathbf{H}_r + \mathbf{H}_{cd} + \mathbf{H}_{op} + \mathbf{H}_{nq} \quad (1)$$

with \mathbf{H}_r and \mathbf{H}_{cd} being the semi-rigid rotor part and \mathbf{H}_{nq} the nuclear quadrupole coupling part as used for Fit A:

$$\mathbf{H}_r = A\mathbf{P}_z^2 + B\frac{1}{4}(\mathbf{P}_+^2 + \mathbf{P}_-^2 + \mathbf{P}_+\mathbf{P}_- + \mathbf{P}_-\mathbf{P}_+) - C\frac{1}{4}(\mathbf{P}_+^2 + \mathbf{P}_-^2 - \mathbf{P}_+\mathbf{P}_- - \mathbf{P}_-\mathbf{P}_+), [43] \quad (2)$$

$$\mathbf{H}_{cd} = -\Delta_J\mathbf{P}^4 - \Delta_{JK}\mathbf{P}^2\mathbf{P}_z^2 - \Delta_K\mathbf{P}_z^4 - \delta_J\mathbf{P}^2(\mathbf{P}_+^2 + \mathbf{P}_-^2) - \delta_{K\frac{1}{2}}\{\mathbf{P}_z^2, (\mathbf{P}_+^2 + \mathbf{P}_-^2)\}, [44] \quad (3)$$

$$\mathbf{H}_{nq} = \mathbf{V}^{(2)} \cdot \mathbf{Q}^{(2)}, \text{ with } \chi_{aa} = 2eQV_0^{(2)}, \chi_{bb} - \chi_{cc} = \sqrt{6}eQ(V_2^{(2)} + V_{-2}^{(2)}). [43] \quad (4)$$

The supplementary \mathbf{H}_{op} part includes odd power order parameters needed to fit the E species separately:

$$\mathbf{H}_{op} = (q + q_J\mathbf{P}^2 + q_K\mathbf{P}_z^2)\mathbf{P}_z + (r + r_J\mathbf{P}^2 + r_K\mathbf{P}_z^2)\frac{1}{2}(\mathbf{P}_+ + \mathbf{P}_-). [18,45] \quad (5)$$

The achieved standard deviation is 4.1 kHz, as shown in Fit E of Table 2 along with the obtained parameters. This consistency is a strong indication that the assignment is correct. Note that the rotational and centrifugal distortion constants are different in Fit A and Fit E because they have become effective and no longer represent the molecular geometry and centrifugal distortion effects. Furthermore, *WS18* applies perturbation theory to treat the ^{14}N nuclear quadrupole coupling effects, and thus, the χ_{ab} parameter cannot be determined in Fit A containing only the torsional ground state lines [43]. We then applied the program *BELGI-C_s-hyperfine* [46,47] to the same data set, aiming to achieve a global fit with measurement accuracy

employing a larger set of adjustable parameters, and succeeded with a root-mean-square deviation of 4.4 kHz for the A and E species fitted together. Not like the *XIAM* code which applies the combined axis method where the internal rotation Hamiltonian of each single rotor is first set up in the rho axis system and then transformed into the principal axis system, the Hamiltonian of the *BELGI-C_s-hyperfine* code is written exclusively in the rho axis system. Therefore, molecular parameters obtained from the two programs are not comparable. The *BELGI-C_s-hyperfine* parameters in the rho axis system and their operators are summarised in Table 4. Parameters transformable into the principal axis system are given in Table 3. We note that this transformation is not possible for all fitted parameters, and currently can only be applied for the rotational constants [48,49] and the NQCCs [13,50], with conversion details given in Refs. [12,51]. A list of all fitted frequencies along with their observed-minus-calculated residuals are collected in Table S5 of the supplementary materials.

Table 2. Molecular parameters of the A and E species fits of *anti*-MVT as obtained with the program *WS18*.

Par. ^a	Unit	Fit A	Fit E
<i>A</i>	MHz	2455.76128(17)	2455.59319(16)
<i>B</i>	MHz	1812.485438(74)	1805.206282(71)
<i>C</i>	MHz	1048.405109(35)	1048.377086(37)
Δ_J	kHz	0.18700(82)	0.02604(90)
Δ_{JK}	kHz	0.0241(33)	0.5429(71)
Δ_K	kHz	0.059(11)	-0.292(20)
δ_J	kHz	0.08213(42)	0.00254(44)
δ_K	kHz	0.3410(18)	0.2065(30)
χ_{aa}	MHz	-3.5556(10)	-3.55099(94)
χ^-	MHz	-1.5434(18)	-1.5558(19)
$ \chi_{ab} $	MHz		1.7806(61)
<i>q</i>	MHz		99.69356(48)
<i>q_J</i>	kHz		-9.510(43)
<i>q_K</i>	kHz		9.758(87)
<i>r</i>	MHz		383.19058(54)
<i>r_J</i>	kHz		-42.256(23)
<i>r_K</i>	kHz		6.93(18)
<i>rms</i> ^b	kHz	3.8	3.1
<i>N</i> ^c		253	270

^a All parameters refer to the principal axis system, Watson's A reduction in the I' representation was used. Note that the off-diagonal term χ_{ab} of the nuclear quadrupole coupling tensor cannot be fitted in Fit A due to the presence of only torsional ground state lines.

^b Standard deviation of the fit.

^c Number of lines.

Table 3. Molecular parameters of *anti*-MVT in the principal axis system obtained by the programs *XIAM* and *BELGI-C_s-hyperfine*.

Par. ^a	Unit	<i>XIAM</i>	<i>BELGI</i>	Calc.
<i>A</i>	MHz	2455.4546(22)	2458.388(15)	2434.9 ^b
<i>B</i>	MHz	1807.82116(96)	1801.74(16)	1804.0 ^b
<i>C</i>	MHz	1048.39859(50)	1048.1408(12)	1047.5 ^b
Δ_J	kHz	0.069(10)		0.20573 ^b
Δ_{JK}	kHz	0.224(47)		0.19091 ^b
Δ_K	kHz	1.09(14)		-0.36947 ^b
δ_J	kHz	0.0204(50)		0.02804 ^b
δ_K	kHz	0.282(24)		0.81755 ^b
ρ	unitless	0.011468 ^c	0.011006(25)	
V_3	cm ⁻¹	107.0901(7)	105.07(12)	105.7 ^d
D_{pi2J}	MHz	-0.15533(39)		
D_{pi2K}	MHz	0.4291(19)		
D_{pi2-}	MHz	-0.13393(44)		
$\angle(i.a)$	deg	100.8894(3)	101.1443(37)	98.29
$\angle(i.b)$	deg	10.8894(3)	11.144(37)	8.36
$\angle(i.c)$	deg	90.00 ^e	90.00 ^e	88.87
χ_{aa}	MHz	-3.545(13)	-3.5790(83)	-3.5525 ^f
χ_{bb}	MHz	0.991(18) ^g	1.0275(82)	1.1313 ^f
χ_{cc}	MHz	2.554(41) ^g	2.552(17) ^g	2.4211 ^f
$ \chi_{ab} $	MHz	1.76(11)	1.747(11)	1.8195 ^f
N_A/N_E ^h		253/270	253/270	
rms ⁱ	kHz	36.5	4.4	

^a All parameters refer to the principal axis system. Watson's A reduction in the I' representation was used.

^b Ground state rotational constants and centrifugal distortion constants obtained from anharmonic frequency calculations at the MP2/6-311++G(d,p) level of theory.

^c Derived parameter.

^d Calculated at the B3LYP-D3BJ/6-311++G(d,p) level of theory.

^e Fixed due to symmetry (see text).

^f Calculated at the B3PW91/6-311+G(d,p)//MP2/6-311++G(d,p) levels of theory, see text.

^g Derived from the obtained parameter $\chi_- = \chi_{bb} - \chi_{cc}$ and $\chi_{aa} + \chi_{bb} + \chi_{cc} = 0$

^h Number of the A (N_A) and the E species lines (N_E).

ⁱ Root-mean-square deviation of the fit.

Table 4. Spectroscopic constants of *anti*-MVT in the rho axis system obtained with the program *BELGI-C_s-hyperfine*.

Operator ^a	Par. ^b	Unit	Value
\mathbf{P}_z^2	A	MHz	1845.99(17)
\mathbf{P}_x^2	B	MHz	2414.1434(11)
\mathbf{P}_y^2	C	MHz	1048.1408(12)
$-\mathbf{P}^4$	Δ_J	kHz	0.107(11)
$-\mathbf{P}^2\mathbf{P}_z^2$	Δ_{JK}	kHz	0.313(46)
$-\mathbf{P}_z^4$	Δ_K	kHz	-0.524(36)
$-2\mathbf{P}^2(\mathbf{P}_x^2 - \mathbf{P}_y^2)$	δ_J	kHz	0.0424(54)
$-\{\mathbf{P}_z^2, (\mathbf{P}_x^2 - \mathbf{P}_y^2)\}^2$	δ_K	kHz	0.289(11)
$\{\mathbf{P}_z, \mathbf{P}_x\}$	D_{ab}	GHz	0.164608(14)
$\{\mathbf{P}_z, \mathbf{P}_x\}[1 - \cos(3\alpha)]$	d_{ab}	GHz	-0.018421(51)
$(1/2)[1 - \cos(3\alpha)]$	V_3	cm ⁻¹	105.07(12)
\mathbf{P}_α^2	F	cm ⁻¹	5.3988 ^c
$\mathbf{P}_z\mathbf{P}_\alpha$	ρ	unitless	0.011006(25)
$[1 - \cos(3\alpha)]\mathbf{P}^2$	F_v	MHz	0.6874(35)
$[1 - \cos(3\alpha)]\mathbf{P}_z^2$	k_5	MHz	7.73(48)
$\mathbf{P}_z\mathbf{P}_\alpha\mathbf{P}^2$	L_v	kHz	-12.85(67)
	$2\chi_{aa}$	MHz	-0.317(13)
	$2\chi_{bb}$	MHz	-4.786(13)
	$2\chi_{ab}$	MHz	-5.332(24)
	rms^d	kHz	4.4
	N_A/N_E^e		253/270

^a Operator which the parameter multiplies in the program. $\{A,B\} = AB + BA$. The product of the parameter and operator from a given row yields the term actually used in the rotation-torsion Hamiltonian, except for F , ρ , and A , which occur in the Hamiltonian in the form $F(\mathbf{P}_\alpha - \rho\mathbf{P}_z^2) + A\mathbf{P}_z^2$.

^b All parameters refer the rho axis system and cannot be directly compared to those referred to the principal axis system.

^c Fixed to the value from *XIAM* fit.

^d Root-mean-square deviation of the fit.

^e Number of the A species (N_A) and the E species lines (N_E).

Discussion

After *anti*-MVT was assigned, only seven weak lines remain in the survey spectrum, i.e. the higher in energy *syn* form is not present with sufficient intensity to be assigned under our jet cooled conditions. The assignment of *anti*-MVT was checked by separate fits. Global fits on a set of 253 A species and 270 E species transitions including hyperfine components were performed using the *XIAM* and *BELGI-C_s-hyperfine* programs. The *XIAM* fit has a standard

deviation of 36.5 kHz, and the program fails to attain the measurement accuracy estimated to be 4 kHz. The *BELGI-C_s-hyperfine* program succeeds to decrease the deviation to 4.4 kHz with additional parameters. Molecular parameters obtained from *BELGI-C_s-hyperfine* are in the rho axis system and cannot be directly compared to those of *XIAM*, given in the principal axis system. After transforming some *BELGI-C_s-hyperfine* parameters from the rho to the principal axis system, the agreement to *XIAM* parameters is fairly well, as shown in Table 3. The NQCC values obtained using *XIAM* and *BELGI-C_s-hyperfine* match very well and they are also close to those obtained using the B3PW91/6-311+G(df,pd)//MP2/6-311++G(d,p) combination.

The equilibrium rotational constants calculated using different combinations of methods and basis sets mentioned in section *Basis set variation* are generally in agreement with the experimental ones with deviations being less than 2 % in all cases. The predicted values obtained using our frequently used levels, MP2/6-311++G(d,p) and B3LYP-D3BJ/6-311++G(d,p), provide a deviation of about 1.2 % for the *A* rotational constants and better than 1 % for the *B* and *C* rotational constants. The ωB97X-D method paired with the 6-311G(d,p), 6-311G+(d,p) and 6-311G++(d,p) basis sets predicts all three rotational constants closest to the experimental values. More generally, the ωB97X-D and M06-2X methods perform very well for *anti*-MVT. The MP2/6-31G(d,p) level, which has been recommended for many aromatic ring molecules, maintains its general reliability also in the present case.

The B3LYP-D3BJ/6-311++G(d,p) level of theory predicts almost the exact value of the experimental barrier height (see Table 3) deduced from a typical three-fold potential curve. In contrast, the MP2/6-311++G(d,p) level yields a value which is only about half of the experimental one. Estimating the methyl torsional barrier with high accuracy using quantum chemical calculations is still difficult, and it is often encountered that the MP2 method underestimates and the B3LYP method overestimates the barrier, as demonstrated for example in 2-methylthiazole [13]. However, our experiments have shown that the values obtained with the B3LYP method is closer to the experimental values in many cases [30,49,52]. In the case of *anti*-MVT, the matching value calculated with B3LYP-D3BJ/6-311++G(d,p) level is probably due to accidental error compensations. Nevertheless, they might be taken into account for initial spectral predictions.

Geometry optimisations using the MP2 method in combination with the 6-311++G(d,p) basis set show that *anti*-MVT has a non-planar structure where the vinyl group is significantly tilted out of the thiazole plane by about 16.3°. Among 97 levels, 8 MP2 levels predict a non-planar structure, reflected by the difference of the tilt angle Θ as given in Table S3 of the supplementary materials. All of them apply Pople's basis set with either (d,p) or (df,pd)

polarisation functions, with or without diffuse functions. The only level of this category which does not predict a significant non-planar structure is the above mentioned MP2/6-31G(d,p) level, though a tiny tilt angle of 0.57° is also observed.

Due to splittings caused by the methyl internal rotation and the nitrogen quadrupole coupling, the intensities of all minor isotopologue lines decrease and their transitions are too weak to be observed in the microwave spectrum. Therefore, it was not possible to determine the microwave structure of *anti*-MVT by isotopic substitutions. To find the answer to the question “planar, or not planar”, we calculated the inertial defect $\Delta_c = -3.322 \text{ u}\text{\AA}^2$ of *anti*-MVT and compared its value with those obtained for other aromatic molecules containing one methyl group. As recently summarized by Buschmann et al., conformers exhibiting C_s symmetry with only two methyl hydrogen atoms with out-of-plane contributions feature an inertial defect of $-3.2 \text{ u}\text{\AA}^2$, with experimental values varying from about $-3.0 \text{ u}\text{\AA}^2$ to $-3.7 \text{ u}\text{\AA}^2$ [53]. The values obtained for the three isomers of methylthiazole are all close to $-3.1 \text{ u}\text{\AA}^2$, i.e. $-3.083 \text{ u}\text{\AA}^2$ for 2-methylthiazole (**1**) [24], $-3.092 \text{ u}\text{\AA}^2$ for 4-methylthiazole (**2**) [54], and $-3.077 \text{ u}\text{\AA}^2$ for 5-methylthiazole (**3**) [55] (for molecule numbers, see Figure 6). The inertial defect of *anti*-MVT was also compared to those calculated using the MP2/6-311++G(d,p) and B3LYP-D3BJ/6-311++G(d,p) levels of theory with the values of $-5.248 \text{ u}\text{\AA}^2$ and $-3.125 \text{ u}\text{\AA}^2$, respectively. The predicted value obtained using the B3LYP-D3BJ method is sufficiently close to the experimental one, indicating the planarity of the heavy atom skeleton of *anti*-MVT.

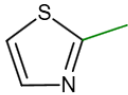
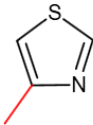
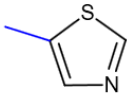
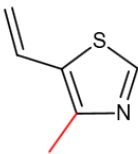

					
	(1)	(2)	(3)	(4)	(5)
V_3 / cm^{-1}	35	358	332	107	127 / 62
$\Delta_c / \text{u}\text{\AA}^2$	-3.083	-3.092	-3.077	-3.323	-6.225
χ_{cc} / MHz	2.390	2.539	2.711	2.551	2.580

Figure 6. Comparison of the inertial defect Δ_c , the ^{14}N NQCC χ_{cc} and the barrier to methyl internal rotation in thiazole derivatives: (**1**) 2-methylthiazole [13], (**2**) 4-methylthiazole [54] (**3**) 5-methylthiazole [55] (**4**) 4-vinyl-5-methylthiazole (this work), and (**5**) 4,5-dimethylthiazole [12].

To support this indication, we compare the experimental ^{14}N NQCC χ_{cc} value of 2.554 MHz achieved with the *XIAM* code with those obtained for other planar thiazole derivatives shown in Figure 6. Since one principal axis of the coupling tensor is collinear with the *c* principal axis with the latter being perpendicular to the thiazole plane, the χ_{cc} values of these molecules can be directly compared. Figure 6 shows that they are very similar, indicating that the electronic surrounding of the nitrogen nucleus is the same for all molecules, thereby supporting the planar structure of MVT. We then tried a fit with the *BELGI-C₁-hyperfine* code to obtain parameters in the rho axis system, which are only used for non-planar structures such as D_{aci} and D_{bci} , multiplying the operators $(\mathbf{P}_x\mathbf{P}_z + \mathbf{P}_z\mathbf{P}_x)$ and $(\mathbf{P}_y\mathbf{P}_z + \mathbf{P}_z\mathbf{P}_y)$, respectively. No significant change was observed for the standard deviation of the fit, and the NQCCs were not well-determined. Altogether, we conclude that at least the structure of *anti*-MVT is effectively planar.

The barrier height to methyl internal rotation of the methyl group of only 107.0901(7) cm^{-1} was obtained with the *XIAM* code. Since the methyl torsional barrier of 4-methylthiazole is 357.6 cm^{-1} [54], we expected a higher value because of steric effects due to the presence of a vinyl group in the neighbourhood of the methyl group. Therefore, the result is rather surprising, but *anti*-MVT is not the first case where steric effects fail to explain the values of methyl torsional barriers. A closely related molecule, 4,5-dimethylthiazole, features a methyl group at the 4- and a methyl group at the 5-position of the thiazole ring with barrier heights of 126.5 cm^{-1} and 61.7 cm^{-1} , respectively [12]. Steric hindrance is inconsistent with these barrier heights which are much lower than those observed for 4- [54] and 5-methylthiazole [55] where the methyl rotor is essentially steric-free. The same situation is observed for the extremely low methyl torsional barrier of 2-methylthiazole [13] (see Figure 6) as well as that of the *o*-methyl group in 2,3-dimethylanisole [11]. The barriers to internal rotation might be lowered by longer C–CH₃ bond and larger C–C–CH₃ angle, but the almost unchanged bond length of 1.50 Å and the very similar angle of about 126° calculated at the MP2/6-311++G(d,p) level of theory cannot explain the drastically different values of the molecule shown in Figure 6. We suspect electrostatic effects due the π -electron delocalisation of the double bonds of the vinyl group and the thiazole ring to be the reason, as suggested in a recent study on 2,3-dimethylfluorobenzene where the methyl group at the 3-position of the phenyl ring seems to be sterically “invisible” to the neighbouring methyl group at the 2-position [10]. Comparison of the barrier to methyl internal rotation thiazole, pyrrole, imidazole, and oxazole derivatives has again confirmed the influence of both steric and electrostatic effects [56]. Extensive theoretical analysis is currently in progress to support this finding from quantum chemical aspects.

Conclusion

The microwave spectrum of the *anti* conformer of MVT was recorded in the frequency range between 2 and 26.5 GHz, revealing splittings consisting of A-E doublets due to internal rotation of the methyl group and hyperfine structures due to the ^{14}N nuclear quadrupole coupling effects. The complex splitting patterns were assigned and fitted first with the *XIAM* code to a standard deviation of 36.5 kHz, then with the *BELGI- C_s -hyperfine* code which reduced this value to 4.4 kHz, close to the measurement accuracy. Separate fits for the A and the E species were also performed to check the line assignments. The torsional barrier of the methyl group is about 107 cm^{-1} , surprisingly low in view of the anticipated steric hindrance caused by the neighbouring vinyl group. A comparison with other thiazole derivatives suggests electrostatic interactions expanded through the π -conjugated system between the vinyl group and thiazole ring to be the reason for the observed value. The barrier height was also compared to values predicted at the MP2/6-311++G(d,p) and B3LYP-D3BJ/6-311++G(d,p) levels of theory where the B3LYP-D3BJ method accidentally calculates almost exactly the methyl torsional barrier. By comparing the inertial defect and the χ_{cc} values of *anti*-MVT with those of other thiazole derivatives, we conclude that the structure of *anti*-MVT is effectively planar, though a number of MP2 levels predict the vinyl group to be tilted out from the thiazole plane.

Disclosure statement

No potential conflict of interest was reported by the authors.

Acknowledgments

S.K. thanks the HRMS committee of the 27th Conference on High Resolution Molecular Spectroscopy, Cologne, 2021, for the opportunity to present the results of this work in an oral contribution. This work was financially supported by the Agence Nationale de la Recherche ANR (project ID ANR-18-CE29-0011). I.K. thanks the Programme National “Physique et Chimie du Milieu Interstellaire” (PCMI) of CNRS/INSU for supporting partly this work.

References

- [1] B. Bak, D. Christensen, L. Hansen-Nygaard and J. Rastrup-Andersen, *J. Mol. Spectrosc.* **9**, 222 (1962).
- [2] B.J. Esselman, M.A. Zdanovskaia, A.N. Owen, J.F. Stanton, R.C. Woods and R.J. McMahon, *J. Chem. Phys.* **155**, 054302 (2021).
- [3] H.V.L. Nguyen and I. Kleiner, *Phys. Sci. Rev.* [Published online] (2021).
<https://doi.org/10.1515/psr-2020-0037>
- [4] S. Khemissi and H.V.L. Nguyen, *ChemPhysChem.* **21**, 1682 (2020).
- [5] J. Mélan, S. Khemissi and H.V.L. Nguyen, *Spectrochim. Acta. A* **247**, 119120 (2021).
- [6] M. Tudorie, I. Kleiner, M. Jahn, J.-U. Grabow, M. Goubert and O. Pirali, *J. Phys. Chem. A* **117**, 13636 (2013).
- [7] L. Ferres, J. Cheung, W. Stahl, H.V.L. Nguyen, *J. Phys. Chem. A* **123**, 3497 (2019).
- [8] T. Nguyen, W. Stahl, H.V.L. Nguyen and I. Kleiner, *J. Chem. Phys.* **154**, 204304 (2021).
- [9] V. Van, W. Stahl and H.V.L. Nguyen, *Phys. Chem. Chem. Phys.* **17**, 32111 (2015).
- [10] S. Khemissi, A. Pérez Salvador and H.V.L. Nguyen, *J. Phys. Chem. A* **125**, 8542 (2021).
- [11] L. Ferres, K-N. Truong, W. Stahl and H.V.L. Nguyen. *ChemPhysChem* **19**, 1781 (2018).
- [12] V. Van, T. Nguyen, W. Stahl, H.V.L. Nguyen and I. Kleiner, *J. Mol. Struct.* **1207**, 127787 (2020).
- [13] T. Nguyen, V. Van, C. Gulté, W. Stahl, M. Schwell, I. Kleiner and H.V.L. Nguyen, *J. Chem. Phys.* **152**, 134306 (2020).
- [14] H. Saal, J.-U. Grabow, A.R. Hight Walker, J.T. Hougen, I. Kleiner and W. Caminati, *J. Mol. Spectrosc.* **351**, 55 (2018).
- [15] A.J. Shirar, D.S. Wilcox, K.M. Hotopp, G.L. Storck, I. Kleiner and B.C. Dian, *J. Phys. Chem. A* **114**, 12187 (2010).
- [16] W. Jäger, Microwave study of atmospheric oxidation product *m*-toluic acid and its monohydrate, <<http://hdl.handle.net/2142/97117>>.

- [17] E.G. Schnitzler, N.A. Seifert, I. Kusuma and W. Jäger, *J. Phys. Chem. A* **121**, 8625 (2017).
- [18] S. Herbers, S.M. Fritz, P. Mishra, H.V.L. Nguyen and T.S. Zwier, *J. Chem. Phys.* **152**, 074301 (2020).
- [19] R. Hakiri, N. Derbel, H.V.L. Nguyen and H. Mouhib, *Phys. Chem. Chem. Phys.* **20**, 25577 (2018).
- [20] V. Van, W. Stahl and H.V.L. Nguyen, *ChemPhysChem* **17**, 3223 (2016).
- [21] C. Dindić, W. Stahl and H.V.L. Nguyen, *Phys. Chem. Chem. Phys.* **22**, 19704 (2020).
- [22] C. Dindić and H.V.L. Nguyen, *ChemPhysChem* **22**, 2420 (2021).
- [23] M.J. Frisch, G.W. Trucks, H.B. Schlegel, G.E. Scuseria, M.A. Robb, J.R. Cheeseman, G. Scalmani, V. Barone, G.A. Petersson, H. Nakatsuji, X. Li, M. Caricato, A.V. Marenich, J. Bloino, B.G. Janesko, R. Gomperts, B. Mennucci, H.P. Hratchian, J.V. Ortiz, A.F. Izmaylov, J.L. Sonnenberg, D. Williams-Young, F. Ding, F. Lipparini, F. Egidi, J. Goings, B. Peng, A. Petrone, T. Henderson, D. Ranasinghe, V.G. Zakrzewski, J. Gao, N. Rega, G. Zheng, W. Liang, M. Hada, M. Ehara, K. Toyota, R. Fukuda, J. Hasegawa, M. Ishida, T. Nakajima, Y. Honda, O. Kitao, H. Nakai, T. Vreven, K. Throssell, J.A. Montgomery, Jr., J.E. Peralta, F. Ogliaro, M.J. Bearpark, J.J. Heyd, E.N. Brothers, K.N. Kudin, V.N. Staroverov, T.A. Keith, R. Kobayashi, J. Normand, K. Raghavachari, A.P. Rendell, J.C. Burant, S.S. Iyengar, J. Tomasi, M. Cossi, J.M. Millam, M. Klene, C. Adamo, R. Cammi, J.W. Ochterski, R.L. Martin, K. Morokuma, O. Farkas, J.B. Foresman and D.J. Fox, , *Gaussian 16* (Gaussian, Inc., Wallingford CT, 2016).
- [24] C. Møller and M. S. Plesset, *Phys. Rev.* **46**, 618 (1934).
- [25] A.D. Becke, *J. Chem. Phys.* **98**, 5648 (1984).
- [26] C. Lee, W. Yang and R.G. Parr, *Phys. Rev. B.* **37**, 785 (1988).
- [27] S. Grimme, S. Ehrlich and L. Goerigk, *J. Comput. Chem.* **32**, 1456 (2011).
- [28] S. Grimme, J. Antony, S. Ehrlich and H. Krieg, *J. Chem. Phys.* **132**, 154104 (2010).
- [29] M.J. Frisch, J.A. People and J.S. Binkley, *J. Chem. Phys.* **80**, 3265 (1984).
- [30] L. Ferres, H. Mouhib, W. Stahl and H.V.L. Nguyen, *ChemPhysChem* **18**, 1855 (2017).
- [31] H.V.L. Nguyen, A. Jabri, V. Van and W. Stahl, *J. Phys. Chem. A* **118**, 12130 (2014).
- [32] T. Yanai, D.P. Tew and N.C. Handy, *Chem. Phys. Lett.* **393**, 51 (2004).

- [33] J.-D. Chai and M. Head-Gordon, *Phys. Chem. Chem. Phys.* **10**, 6615 (2008).
- [34] Y. Zhao and D.G. Truhlar, *Theor. Chem. Acc.* **120**, 215 (2008).
- [35] R.J. Bartlett and M. Musial, *Rev. Mod. Phys.* **79**, 291 (2007).
- [36] T.H. Dunning Jr., *J. Chem. Phys.* **90**, 1007 (1989).
- [37] R.A. Kendall, T.H. Dunning Jr. and R.J. Harrison, *J. Chem. Phys.* **96**, 6796 (1992).
- [38] R. Kannengießer, W. Stahl, H.V.L. Nguyen and W.C. Bailey, *J. Mol. Spectrosc.* **317**, 50 (2015).
- [39] W.C. Bailey, *J. Chem. Phys.* **252**, 57 (2000).
- [40] J.-U. Grabow, W. Stahl and H. Dreizler, *Rev. Sci. Instrum.* **67**, 4072 (1996).
- [41] J.-U. Grabow and W. Stahl, *Z. Naturforsch.* **45a**, 1043 (1990).
- [42] H. Hartwig and H. Dreizler, *Z. Naturforsch.* **51a**, 923 (1996).
- [43] W. Gordy and R.L. Cook, *Microwave molecular spectra*, Vol. 18, 3rd Ed., Wiley, New York, 1984.
- [44] J.K.G. Watson, in: J.R. Durig (Ed.), *Vibrational Spectra and Structure*, Eslevier Scientific Publishing Company, 1977.
- [45] N. Ohashi, J. Hougen, R. Suenram, F. Lovas, Y. Kawashima, M. Fujitake, and J. Pyka, *J. Mol. Spectrosc.* **227**, 28 (2004).
- [46] J.T. Hougen, I. Kleiner and M. Godefroid, *J. Mol. Spectrosc.* **163**, 559 (1994).
- [47] R. Kannengießer, W. Stahl, H.V.L. Nguyen and I. Kleiner, *J. Phys. Chem. A* **120**, 3992 (2016).
- [48] K. Eibl, W. Stahl, I. Kleiner and H. V. L. Nguyen, *J. Chem. Phys.* **149**, 144306 (2018).
- [49] L. Ferres, W. Stahl, I. Kleiner and H.V.L. Nguyen, *J. Mol. Spectrosc.* **343**, 44 (2018).
- [50] T. Nguyen, C. Dindic, W. Stahl, H.V.L. Nguyen and I. Kleiner, *Mol. Phys.* **118**, 1668572 (2020).
- [51] D. Jelisavac, D. C. Cortés-Gómez, H. V. L. Nguyen, L. W. Sutikdja, W. Stahl and I. Kleiner, *J. Mol. Spectrosc.* **257**, 111 (2009).
- [52] L. Ferres, W. Stahl and H.V.L. Nguyen, *J. Chem. Phys.* **148**, 124304 (2018).

- [53] P. Buschmann, K.G. Lengsfeld, J. Djahandideh and J.-U. Grabow, *J. Mol. Struct.* **1250**, 131805 (2020).
- [54] W. Jäger and H. Mäder, *Z. Naturforsch.* **42a**, 1405 (1987).
- [55] W. Jäger and H. Mäder, *J. Mol. Struct.* **190**, 295(1988).
- [56] T. Nguyen, W. Stahl, H.V.L. Nguyen and I. Kleiner, *J. Mol. Spectrosc.* **372**, 111351 (2020).